Steel and Composite Structures, *Vol. 33, No. 4* (*2019*) *537-550*
DOI: https://doi.org/10.12989/scs.2019.33.4.537

Reinforcement design of the top and bottom slabs of composite box girder with corrugated steel webs

Hu Zhao*[1], Hongye Gou [2a], Ying-Sheng Ni [3b] and Dong Xu [4c]

[1] *China Railway Siyuan Survey and Design Group CO., LTD, Wuhan, Hubei province, 430063, P.R. China*
[2] *Department of Bridge Engineering, School of Civil Engineering, Southwest Jiaotong University, Chengdu, Sichuan province,611756, P.R. China*
[3] *Research Institute of Highway Ministry of Transport, M.O.T, Beijing, 100088, P.R. China*
[4] *Department of Bridge Engineering, Tongji University, Shanghai, 200092, P.R. China*

(*Received June 22, 2019, Revised September 8, 2019, Accepted October 8, 2019*)

Abstract. Korea and Japan have done a lot of research on composite girders with corrugated steel webs and built many bridges with corrugated steel webs due to the significant advantages of this type of bridges. Considering the demanding on the calculation method of such types of bridges and lack of relevant reinforcement design method, this paper proposes the spatial grid analysis theory and tensile stress region method. First, the accuracy and applicability of spatial grid model in analyzing composite girders with corrugated steel webs was validated by the comparison with models using shell and solid elements. Then, in a real engineering practice, the reinforcement designs from tensile stress region method based on spatial grid model, design empirical method and specification method are compared. The results show that the tensile stress region reinforcement design method can realize the in-plane and out-of-plane reinforcement design in the top and bottom slabs in bridges with corrugated steel webs. The economy and precision of reinforcement design using the tensile stress region method is emphasized. Therefore, the tensile stress region reinforcement design method based on the spatial grid model can provide a new direction for the refined design of composite box girder with corrugated steel webs.

Keywords: corrugated steel webs; composite girder bridge; grid reinforcement; tensile stress region; spatial grid analysis theory

1. Introduction

The composite girder bridges with corrugated steel webs have advantages such as light weight, low cost, beautiful appearance, and conforming to the national conditions of China at present, so they are popular with the builders increasingly. Countries such as Korea and Japan have done a lot of research on the composite girder with corrugated steel webs and built various types of bridges. Japan has applied and built the most composite girder with corrugated steel webs, up to more than 200 bridges. In China, nearly 50 bridges with corrugated steel webs have been constructed and are under construction. The application of corrugated steel webs has developed from the simply-supported and continuous girder bridges to the continuous rigid frame and cable stayed bridges now. Meanwhile, the cross section also extends from the single-box single-cell to single-box multi-cell and multi-box multi-cell. Most typical examples include the Guoshoujing Bridge and Gangtielu Bridge in Baiquan Avenue of Xingtai, Hebei (the first one-box-seven-cell composite box girder bridge with corrugated steel webs in China), (70 + 11 × 120 + 70) m prestressed concrete continuous box girder with corrugated steel webs of Yellow River Bridge in Juancheng of Shandong province, and (60 + 5 × 120 + 60) m multi-tower composite girder cable stayed bridge with corrugated steel webs of Chaoyang Bridge (Ma 2017). Typical arrangement of composite girder bridges with corrugated steel webs is shown in Fig. 1.

At present, the analysis and reinforcement design of composite girder bridges with corrugated steel webs in China refer to *Design and Construction Specifications for Prestressed Concrete Bridge with Corrugated Steel Webs* in Japan, the regional standard of Guangdong Province –

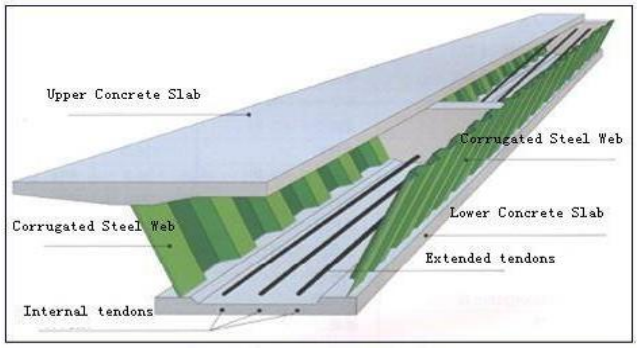

Fig. 1 Typical corrugated steel web bridge

*Corresponding author, Ph.D.,
E-mail: whzhh123@126.com
[a] Professor, E-mail: gouhongye@swjtu.edu.cn
[b] Ph.D., E-mail: niyingsheng2008@aliyun.com
[c] Professor, E-mail: Xu_dong@tongji.edu.cn

ISSN: 1229-9367 (Print), 1598-6233 (Online)

Technical Regulations for Prestressed Concrete Box Girder Bridge with Corrugated Steel Webs, and the regional standard of Henan Province – *Technical Specifications for Highway Prestressed Concrete Box Girder Bridge with Corrugated Steel Webs*, etc. There is no unified specification yet in China, so the analysis and reinforcement design of the top and bottom slabs of bridges with corrugated steel webs still adopt the single section method in the bridge specification (Xu *et al*. 2015).

The analysis of bridge structures generally adopts the Finite Element Models (FEM) of different complexity levels. Such FEMs (Pipinato 2016) may include spine models (simple), grillage models (moderate) and FEMs using shell or solid elements (sophisticated). However, the spine models cannot accurately analyze bridges with significant space effects. These spatial effects include the shear lag effect in the flanges, the ununiform load distribution in the cross section due to eccentric loads, the plane section assumption in wide bridges. Due to inherent imperfection, the grillage models cannot accurately reflect the shear stress flow in box sections and the local stress distribution in top and bottom slabs. Compared to the straightforward and intuitive internal forces result in spine or grillage models, the result of FEMs using shell or solids elements is hard to directly applied in the reinforcement design. These sophisticated models are normally used to check the local effects while the spine and the grillages models are used in the overall analysis of the structures (Ma *et al*. 2017).

At the same time, in the calculation stress, for a complex bridge, the stress effect of the structure under external load needs focusing on the upper edge, lower edge and in-plane principal stresses of each plate (top plate, bottom plate and web), rather than being simply expressed by the upper and lower edge stress of section respectively representing the upper edge of top plate and the lower edge of bottom plate as the calculation stress, so as to embody the stress conditions and possible cracking situations of the position by the corresponding calculation stress, and also reflect the complex stress conditions of such bridge structure more accurately.

Hence, it is necessary to propose a new structural analysis method to accurately obtain the internal forces and stresses as well as put forward a new reinforcement method for PC box girder bridges with corrugated steel webs. In view of this, (Ma *et al*. 2017, Xu *et al*. 2017) describes and applies the practical refinement analytical method – spatial grid model. The tensile stress region method is used to gain the principal stresses with spatial grid model as the carrier and accordingly realize the refined calculation and reinforcement design of plates. The grid model treats the composite girder section as being composed of several plates, makes the girder grillage division for each plate, and equivalently replaces each plate by the cruciform grillage.

Compared with the grillage models, the spatial grid models are better in these ways: (1) The dense division of the top slabs enables the acquirement of accurate stress distribution in the top slabs without the need to calculate the effective width; (2) The spatial grid models are able to accurately simulate the torsion of box sections. The torsion is reflected by the shear stresses of each girder grillage through the mutually combined action in different grids; (3) The distortion and the lateral bending behavior of the cross section under external loads can be well captured; (4) It can analyze various deformation of the composite girder section under the eccentric load.

Apart from these advantages, the output of the spatial grid model is in the form of internal forces, stresses and displacements. Hence, the structural state (forces, stresses) of different components can be obtained conveniently and reinforcement design could be carried out correspondingly, which has important significance in the design analysis of the practical engineering (Ma *et al*. 2017, Xu *et al*. 2015).

2. The spatial grid model

In structural analysis, the complex bridge structure can be decomposed into several plates. Each plate element is composed of a cruciform grillage composed of 6 DOF beam element. The stiffnesses of these beams are taken using the principle of equivalent rigidity to that of the plate (seen in Fig. 2). The quantity of plates constituting the bridge is equal to the number of cruciform grillage. Therefore, the bridge structure can be treated as a spatial grid model. As shown in Fig. 2, the cross section of the single box girder can be decomposed into a top plate, a bottom plate and two webs. The cruciform grillages in different planes assemble the box girder as a spatial net structure, which is termed as spatial grid model (Xu *et al*. 2017).

2.1 Mesh of the spatial grid model

In the spatial grid model, the longitudinal girder can be meshed in accordance with the usual meshing rules for spine model. The refinement degree of the mesh for the

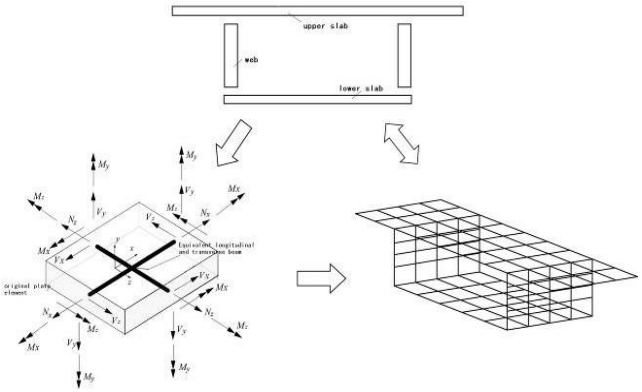

Fig. 2 Schematic show of spatial grid model

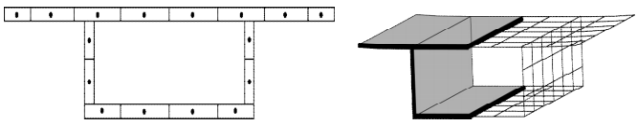

Fig. 3 Structure partitioning for box girder bridge in spatial grid model

cross section of girder should be determined in accordance with the cross section and modelling requirements to reflect the space effect. An example of the mesh for spatial grid model is shown in Fig. 3.

2.2 Cross section property for spatial grid model

In the spatial grid model for the box girders with webs, the cross section mainly includes three types: (1) the integral web part, (2) partitioned parts of web, and (3) partitioned parts of top and bottom plates, as shown in Fig. 4. The calculation of these cross sections and properties is consistent with the cross section properties of traditional beam elements, which is calculated by the actual cross sectional dimension after mesh (Ma *et al*. 2017).

A common rectangular section after mesh (Fig. 5) is taken as an example to show the calculation of the cross section property of typical parts in the spatial grid model.

Axial area

$$A_x = bh \tag{1}$$

Shear area

$$A_y = A_z = bh \tag{2}$$

Bending moment of inertia

$$I_z = \frac{b^3 h}{12}; \qquad I_y = \frac{bh^3}{12} \tag{3}$$

Torsional moment of inertia

$$I_T = \frac{4 I_z I_y}{\beta (I_z + I_y)}; \quad \beta = 1.3\sim1.6 \tag{4}$$

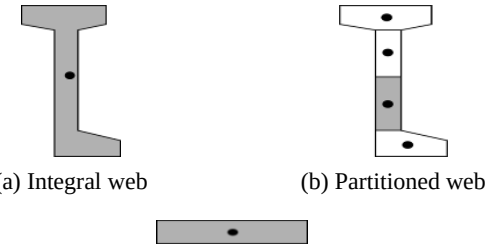

(a) Integral web (b) Partitioned web

(c) Partitioned parts of top and bottom plates

Fig. 4 Typical cross section in spatial grid model

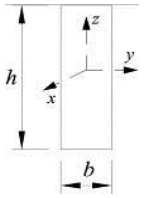

Fig. 5 Calculation of common cross section characteristics in spatial grid model

2.3 Analysis and modelling in spatial grid model

In the spatial grid model, the composite beam section was separated into several plates and these plates are replaced by cruciform grillages. Due to the dense division of the top plate, it can analyze the the shear lag effect of the top plate without calculating the effective width. The torsion rigidity is reflected on the shear stress of each beam grillage through the mutual interaction between spatial grids. It can achieve the distortion analysis of the cross section and the transverse flexural deformation of each plate. Meanwhile, it is able to provide a comprehensive deformation analysis of the composite girder under eccentric load (Xu *et al*. 2017).

While using the spatial grid model, the load effect of the cross section can be resisted respectively as: (1) The longitudinal effect of the box girder cross section (such as the axial force and bending moment) is resisted by longitudinal beam; (2) The transverse effect of the box girder cross section (such as the distortion and transverse effect of live load) is sustained by transverse beam; and (3) The torsion effects of the box girder cross section are transformed into shear force of the web beam grillage.

In the spatial grid model, the internal forces of the cross section are distributed among different components according to their stiffnesses. As shown in Fig. 6, a typical cruciform grillage is normally subjected to axial forces N_x and N_y, in-plane shear forces V_{xy} and V_{yx}, and out-of-plane bending moment M_x and M_y. Under N_x and N_y, the in-plane membrane stress is distributed uniformly over the element thickness. The local load effect in top and bottom plates can be calculated as bellow (Ma *et al*. 2017, Ko *et al*. 2013).

The out-of-plane normal stress under M_x and M_y is given as bellow.

$$\sigma_x = \frac{M_y z}{I_y} \tag{5}$$

$$\sigma_y = \frac{M_x z}{I_x} \tag{6}$$

where σ_x and σ_y are normal stresses of the cross section under M_x and M_y respectively; z is the perpendicular distance to the neutral axis; I_x and I_y are second moment of area about the neutral axis x and y, respectively; and M_x and M_y are the bending moment about the neutral axis x and y, respectively.

The in-plane normal stress can be calculated as

$$\sigma_{x-m} = \frac{N_x}{A_x} = \frac{N_x}{b_x h_x} \tag{7}$$

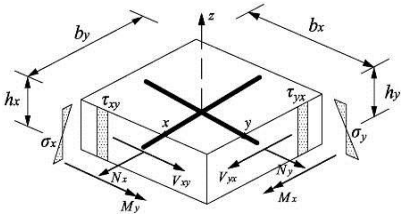

Fig. 6 Calculation of internal forces of elements in spatial grid model

$$\sigma_{y-m} = \frac{N_y}{A_y} = \frac{N_y}{b_y h_y} \tag{8}$$

where $\sigma_{x\text{-}m}$ and $\sigma_{y\text{-}m}$ are the in-plane membrane stress in x and y direction, respectively; and b_x and b_y, h_x and h_y are the width and the height of the element in x and y directions, respectively.

The in-plane shear stress can be derived by

$$\tau_{xy} = \frac{V_{xy}}{b_x h_x} \tag{9}$$

and the in-plane principal tensile stress σ_t and

compressive stress σ_c are derived by the following equation.

$$\frac{\sigma_t}{\sigma_c} = \frac{\sigma_{x-m} + \sigma_{y-m}}{2} \pm \sqrt{\left(\frac{\sigma_{x-m} - \sigma_{y-m}}{2}\right)^2 + \tau_{xy}^2} \tag{10}$$

The output of the spatial grid model is in the form of internal forces, stresses and displacements of each beam grillage. The stress state of various structural components can be conveniently and accurately obtained. The significance of these output in the practical engineering design is that they could be directly linked to the reinforcement design in agreement with common codes (Shon *et al.* 2015, Elkawas *et al.* 2018, Jiao *et al.* 2017, Hassanein and Kharoob 2017, Li and Wang 2013, Ko *et al.* 2013, Zevallos *et al.* 2016).

2.4 Application scope

The plate elements in spatial grid model provides unique bending, torsion and shear resistance resulting from the integral box cross section girder. These plates can be steel, concrete, or other composite materials such as steel concrete composite beam. The applicability of spatial grid model is not limited to specific structure form and it can be applied to various bridges including the curved, wide, and composite bridges (Chao and Xu 2012, Xu and Yu 2012 Liu *et al*. 2015, Elkawas *et al.* 2017).

3. Parameter analysis and model verification

Through the analysis and comparison (the spatial grid model and FEM model using solid elements) of the simply supported corrugated steel web concrete composite box beam, the rationality of the parameter value and the accuracy of the analysis results for the spatial grid model in the analysis and application of the corrugated web bridge (Elkawas *et al.* 2018).

3.1 Finite element model specification

The comparison is carried out using a 20-m simply-supported composite box girder with corrugated steel web. The top and bottom slabs of the bridge use C50 concrete

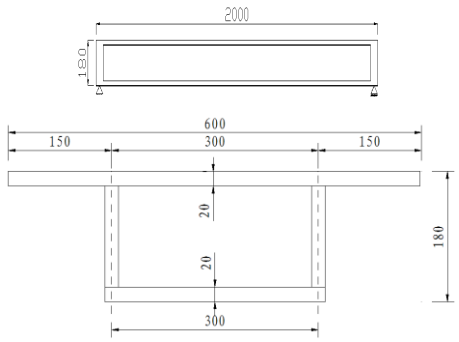

Fig. 7 Elevation and sectional view of the composite box girder with corrugated steel web (Unit: cm)

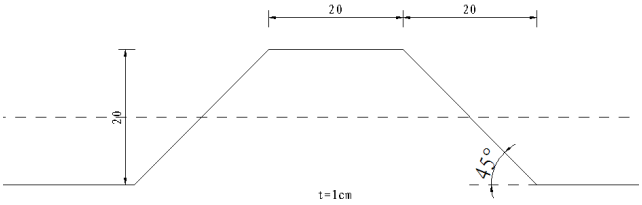

Fig. 8 Dimensions of the corrugated steel web (Unit: cm)

(elastic modulus of 3.45E4MPa, gravity of 26 kN/m^3, and Poisson's ratio of 1/6) while the web uses KL400 steel plate (elastic modulus of 2.0E5MPa, density of 78.5 kN/m^3, and Poisson's ratio of 0.3). See Figs. 7~8 for the dimension of each part in the girder. The thickness of the steel web is 1 cm. The corrugated steel web is built by adopting the actual shape, and the central position coincides with the original web position (Xu *et al*. 2017).

(1) Model specification of the FEM using shell and solid elements

The general-purposed finite element analysis software ANSYS is adopted for the sophisticated FEM. The shell element SHELL63 is used to simulate the corrugated steel web, and the solid element Solid45 is used to simulate the top and bottom concrete slabs. See Fig. 9 for the transverse section and the full-span grid division section in (Lopes *et al.* 2017).

Boundary conditions: Under gravity, the constraint is applied at two sides of the transverse section, and the bottom plate node below the center of the corrugated web. At one end longitudinally, it constrains three direction degrees of freedom UX/UY/UZ of the node, and at the other end, it constrains UY/UZ. Under the effect of anti-symmetric load and eccentric load, it constrains three direction degrees of freedom UX/UY/UZ for the above four nodes.

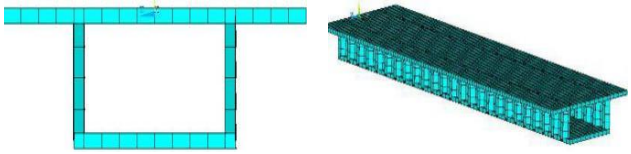

Fig. 9 Finite element model using shell and solid elements

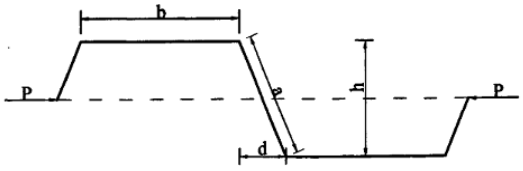

Fig. 10 Schematic diagram of geometrical parameters of gorrugated web

(2) Model specification of the spatial grid model

While simulating the corrugated steel web by the spatial grid model, it is necessary to modify some cross section properties of the elements to match the structural behavior of the corrugated steel webs. The parameter correction mainly lies in the longitudinal and the vertical elements simulating the corrugated steel webs.

In the spatial grid model, the corrugated steel web is modelled as a plane steel plate with equal height and thickness. To accommodate the accordion effect of corrugated steel webs, it is viable to make a reduction of the longitudinal elastic modulus of the plane steel plate (Chen *et al*. 2018, Gajdzicki *et al* 2018). The reduced elastic modulus is noted as the effective elastic modulus *Ex*.

The effective elastic modulus *Ex* is determined by the principal that the original corrugated steel web and the plane steel plate have identical axial deformation under the same axial load P, as shown in Fig. 10.

The axial deformation of the corrugated steel web under the axial force P is obtained from Castigliano theorem, i.e.

$$\delta_1 = \frac{P}{6E_0 I}\left(\frac{a^3}{2} + 3h^2 b\right) \tag{11}$$

The axial deformation of the plane steel plate under the axial force P is given as

$$\delta_2 = \frac{2P}{E_x A}(b + d) \tag{12}$$

Imposing $\delta_1 = \delta_2$ leads to the effective elastic modulus E_x

$$Ex = \frac{E_0(b+d)}{a^3/2h^2 + 3b} \cdot \frac{t^2}{h^2} = E_0 \cdot \alpha \cdot \frac{t^2}{h^2}$$

where

$$\alpha = \frac{b+d}{a^3/2h^2 + 3b}, \quad I = t^2 \cdot A/12,$$

A is the cross sectional area of steel plate.

The effective elastic modulus E_x for the axial direction of corrugated steel web is generally less one hundredth and even less one thousandth of the elastic modulus E_0 of the plane steel plate. This means that the accordion effect of the corrugated steel web makes the axial rigidity very small. Hence, the axial forces contributed from the corrugated steel webs hardly contribute to the bending moment and axial force of the whole cross section.

Regarding the structure depicted in Fig. 7, the ratio between the effective elastic modulus and the real one, E_x/E_0, is 1/883 using the theoretical formula above.

The above theoretical calculation is verified upon using the sophisticated FEM established by ANSYS. While applying the tensile force and stress, calculate the specific value of the corrugated web and plain plate displacement under the effect of the same axial force. The result shows that the displacement of the corrugated web is 883 times the plain plate displacement, thus it can be seen that the above formula is valid and applicable.

In the spatial grid model, the area of the longitudinal elements for the corrugated steel webs is reduced to 1/883 of the one calculated from Eq. (1). Other geometrical characteristics and material parameters are not modified.

In the spatial grid model, the division spacing of the cross section in the transverse direction is 0.3 m for the top and bottom plates, and is 0.2 m for the web. The division spacing of the longitudinal elements is 0.2 m. The cross section of the vertical bar unit of web is two cross section types as shown in Fig. 11. The corresponding cross section of the vertical bar unit of web selected by the out-plane rigidity is shown as Fig. 12.

The spatial grid model (Fig. 13) for this structure has 9450 elements and 10396 nodes. The top plates, bottom plates and the webs are divided into 22 longitudinal beams (No. T1 ~ T22), 12 longitudinal beams (No. B1 ~ B12) and 7 longitudinal bands (No. W1 ~ W7), respectively. The box beam is divided into 100 segments in the longitudinal direction, each with the length of 0.2 m. The web elements and the flange elements are linked by vertical elements. The loads between the webs and the flanges are transferred by these vertical elements . The boundary conditions of the spatial grid model is identical to those applied in the sophisticated FEM using shell and solid elements in ANSYS.

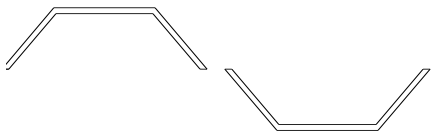

Fig. 11 Cross section of vertical bar unit

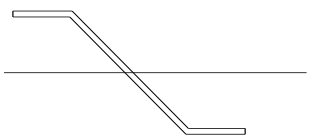

Fig. 12 Out-plane rigidity cross section of vertical bar unit

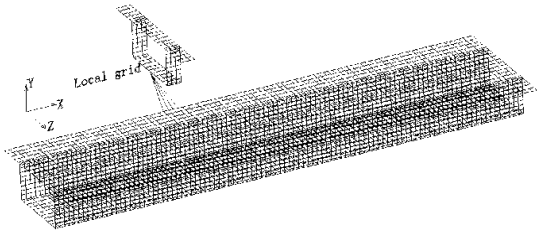

Fig. 13 Schematic diagram of spatial grid model

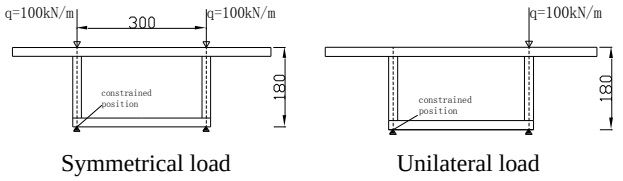

Symmetrical load Unilateral load

Fig. 14 Schematic diagram of loading

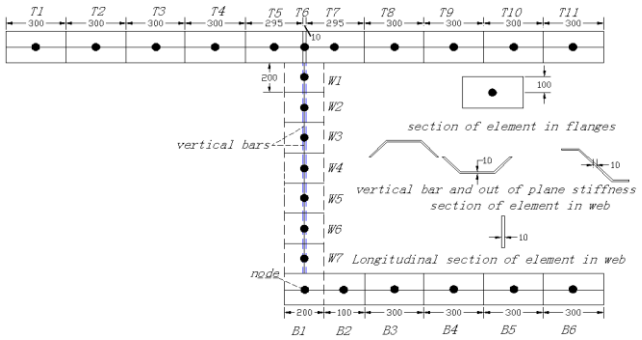

Fig. 15 Position of result comparison point (Unit: mm)

(3) Loading case

The shear lag effect obtained by the spatial grid model and the FEM using shell and solid elements are compared under the loading case of self-weight. Regarding the thin-wall effect (Tomàs *et al*. 2018), the statically indeterminate shear stress distribution and warping normal stress distribution on the cross section are compared under an anti-symmetric load (q = 100 kN/m) and an eccentric load (q = 100 kN/m), as shown in Fig. 14.

(4) Comparative study

The displacements from the two models are extracted and compared. The concerned locations include the left of the top slabs, the middle of the top slab, the middle of the bottom slab and the middle of the web, as shown in Fig. 15. Meanwhile, the normal stresses and the shear stresses are compared at the one-fourth point and the mid span in the longitudinal direction.

Fig. 16 shows the comparison of vertical deflection for the position of four longitudinal bands (T1, W4, T11 and B6) along the direction of the span under gravity. Fig. 17 shows the comparison of vertical deflection for the mid-span and the one-fourth point in the transverse direction under self-weight. Fig. 18 shows the comparison of deformation for the mid-span and the one-fourth point in the transverse direction under the effect of anti-symmetric load. Fig. 19 shows the comparison of deflections for the mid-span and the one-fourth point in the transverse direction under the effect of eccentric load. The digits in the bracket indicate the result from the FEM using shell and solid elements. The maximum differences of the vertical displacements of the longitudinal bands T1, T11, B6 and W4 in two models under gravity are 0.1 mm, 0.15 mm, 0.12 mm and 0.11 mm in Fig. 16, respectively. The maximum differences of the vertical displacement of the two models at the mid-span and the one-fourth point in the transverse direction under gravity are respectively 0.04 mm and 0.05

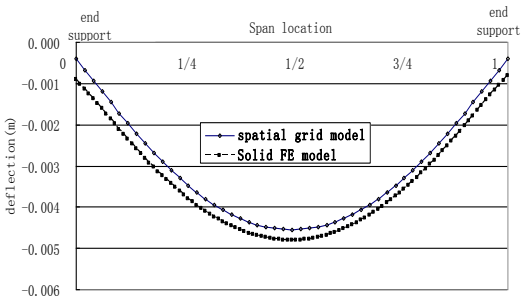

(a) Band T1

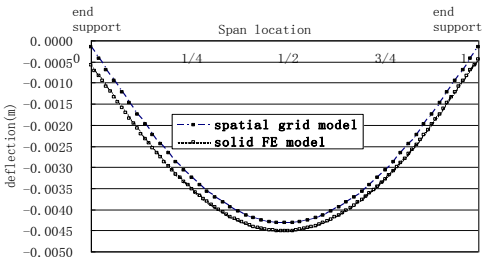

(b) Band T11

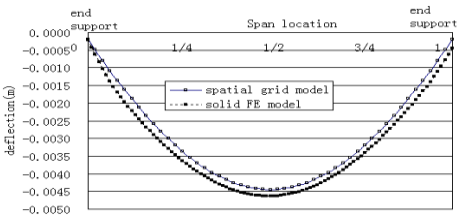

(c) Band T6

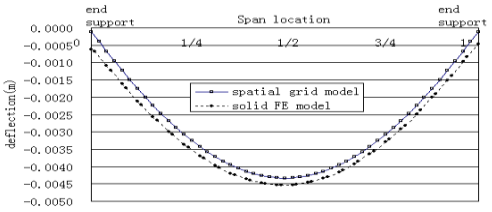

(d) Band W4

Fig. 16 Comparison of vertical deflection under gravity (Unit: m)

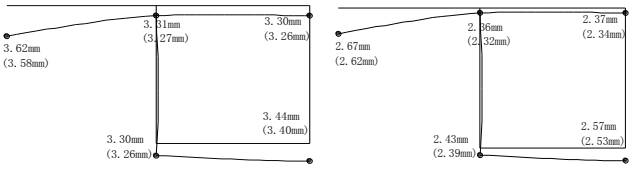

(a) Mid-span position (b) One-fourth position

Fig. 17 Comparison of vertical deflection of transverse section under gravity (Unit: mm)

mm in Fig. 17. The maximum differences of the vertical displacement of the two models at the mid-span and the one-fourth point in the transverse direction under the effect of anti-symmetric load are respectively 0.04 mm and 0.03 mm in Fig. 18. The maximum differences of the vertical

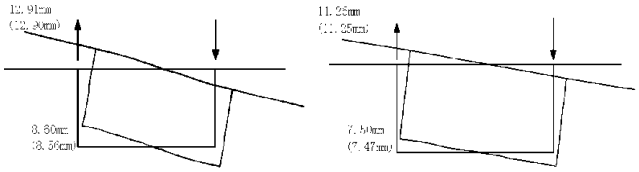

(a) Mid-span position (b) One-fourth position

Fig. 18 Comparison of vertical deflection of transverse section under effect of anti-symmetric load (Unit: mm)

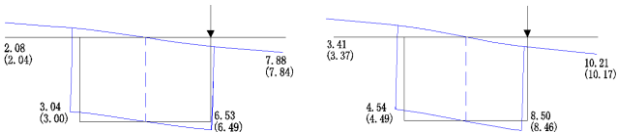

(a) Mid-span position (b) One-fourth position

Fig. 19 Cmparison of vertical deflection of transverse section under effect of eccentric load (Unit: mm)

displacement of two models at the mid-span and the one-fourth point in the transverse direction under the effect of eccentric load are respectively 0.04 mm and 0.05 mm in Fig. 19. Thus, it can be judged that the spatial grid model accurately simulates the structural rigidity.

The normal stresses in the middle-plane spatial grid unit mainly arises from axial force, bending moment and cross section torsion. Here, the normal stress in the position of 0.1 m away from the upper edge of the top plate and bottom plate is valued as the normal stress of the middle-plane plate unit for comparison. Fig. 20 shows the comparison of the normal stress (positive for tensile stresses) of the mid-span and the one-fourth point transverse section under gravity.

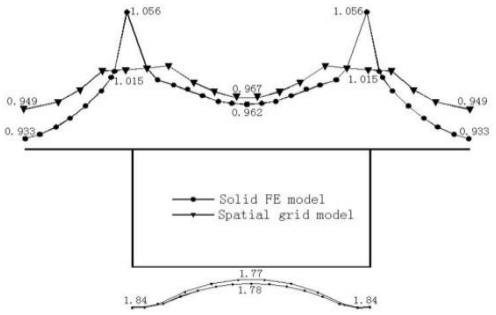

(a) Mid-span position

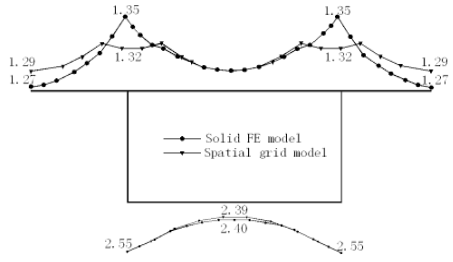

(b) One-fourth position

Fig. 20 Comparison of normal stress of box beam cross section under gravity (Unit: MPa)

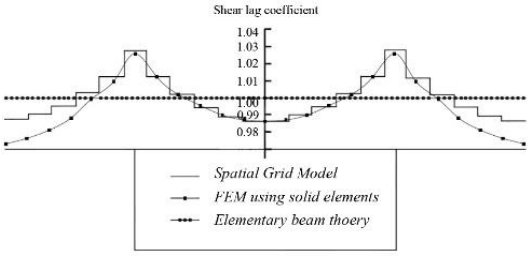

(a) Mid-span position

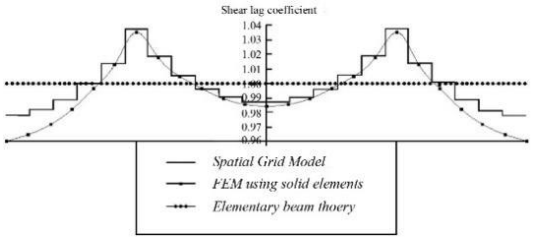

(b) One-fourth position

Fig. 21 Comparison of shear lag effect coefficient of box beam top plate under gravity

From the figure, it can be seen that the variation rule of the Figs. 22~23 show the comparison of warping normal stress (positive for tensile stresses) of mid-span and the one-fourth point transverse section under the effect of anti-symmetric load and eccentric load. In the figure, the result of the solid finite element model is indicated by the dotted line, and the calculation result of the grid model is indicated by the stair-step solid line. From the figure, it can be seen that the stress in the cantilever end of the mid-span and the one-fourth point section is the maximum with the differences of 0.12 MPa and 0.11 MPa respectively, and the stress in the center line of the box beam is the minimum with the difference of nearly zero when the structure is subjected to anti-symmetric load. The stress at the side of eccentric load is the relatively big, and the stress in the cantilever end of the

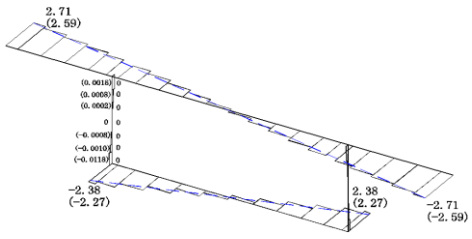

(a) Mid-span position

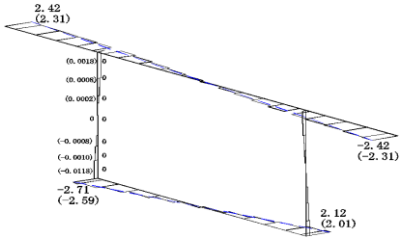

(b) One-fourth position

Fig. 22 Comparison of warping normal stress of box beam cross section under effect of anti-symmetric load

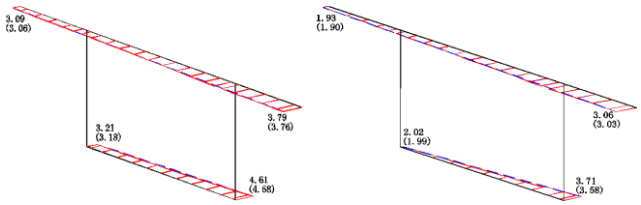

(a) Mid-span position (b) One-fourth position

Fig. 23 Comparison of warping normal stress of box beam cross section under effect of eccentric load

mid-span and the one-fourth point section is the maximum with the differences of 0.03 MPa and 0.03 MPa respectively, and the linear distribution along the top and bottom plates laterally when the structure is subjected to eccentric load. Under the effect of anti-symmetric load and eccentric load, the normal stress of the web is nearly zero. Thus, it is concluded that the calculation results of the FEM using shell and solid elements and the spatial grid model under different loading cases are almost identical. The spatial grid model can accurately simulate the warping effect of the box beam cross section.

Fig. 24 shows the comparison of the shear stresses in the one-fourth position of the simply supported box beam. The shear stresses in the top and bottom slabs is taken at the middle plane of the plate in thickness direction. The result of the FEM using shell and solid elements is indicated by the dotted continuous solid line while the result of the spatial grid model is indicated by the continuous solid line with triangle. From the figure, it can be seen that the top and bottom slabs sustain very small shear stress compared with the web under the loading cases of self-weight, anti-symmetric load and eccentric load, accounting for about 4% of the shear stresses of the web. The webs almost sustain all shear forces. It is consistent with the conclusion in the literatures (Shon *et al.* 2015, Elkawas *et al.* 2018, Jiao *et al.* 2017). The shear stress distribution predicted by two models is very close. In all the analyzed loading cases, for the shear stress distribution in the top and bottom plates, the slight differences in the joint of the web and top and bottom plates can be neglected, because it does not consider the contribution of shearing resistance in the top and bottom plates during calculating. The maximum difference of the shear stress on the steel web is generated from the anti-symmetric load, and is only 1 MPa, accounting for 6% of the stresses obtained from the FEM using shell and solid elements, with very small influence.

In this section, a composite girder bridge with corrugated steel webs is simulated and analyzed by the spatial grid model. The stresses, displacements result are compared with the FEM using shell and solid elements in ANSYS. The high agreement between the results from the two models indicate that the spatial grid model can completely simulate the structural behavior of composite girders with corrugated steel webs, and also can fully correspond to the calculation index of design specifications. It lays a good foundation for the reinforcement design method of composite girder with corrugated steel webs using the tensile stress region method, which will be introduced subsequently.

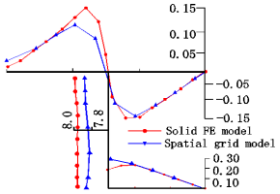

(a) Under the self-supporting effect

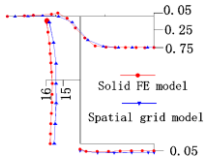

(b) Under the effect of anti-symmetric load

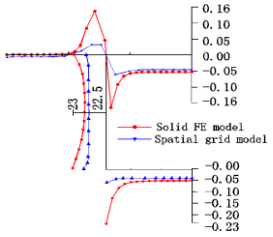

(c) Under the effect of eccentric load

Fig. 24 Comparison of shear stress at the one-fourth position

4. Tensile stress region method

Tensile stress region reinforcement design theory firstly classifies different components in the bridge into two types according to the stress states in these components. The first type relates to plates subjected to in-plane biaxial stresses while the second type relate to girders subjected to the out-of-plane bending moments. The former represents the overall effect of the structure with in-plane stress direction (Fig. 25(a)), and the latter represents the local effect of the structure with out-of-plane stress direction (Fig. 25(b)). The girder subjected to the out-of-plane stresses connects with current specifications, and applies to all clauses about simple bending normal section design state, reinforcement method and design safety in current specifications. Therefore, plates subjected to in-plane biaxial stresses

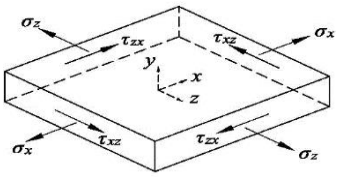

(a) A plate subjected to in-plane biaxial stresses

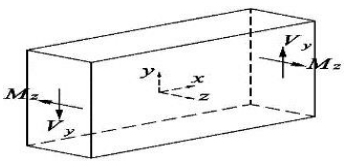

(b) Beams subjected to out-of-plane single stress

Fig. 25 Two types of structure according to stress states

representing the overall effect of the structure is the only prototype component in the tensile stress region reinforcement design method (Xu and Yu 2012). In plates subjected to in-plane biaxial stresses, the normal and the shear stresses are uniformly distributed along the thickness direction, so the in-plane principal stresses are also uniformly distributed along the thickness direction. Hence, such plates can be regarded as membrane members. The region bearing the uniform principal tensile stresses in the membrane plates can be defined as tensile stress region.

5. Tensile stress region reinforcement method for top and bottom slabs of composite girder with corrugated steel webs

In the tensile stress region, when the principal tensile stress is less than the tensile strength of concrete, the concrete mainly bears the principal tensile stress. When the principal tensile stress exceeds the tensile strength of concrete, the concrete cracks and the capacity of bearing the principal tensile stress is greatly weakened. As a result, the principal tensile stress will be sustained by the rebars in the proximity. In other words, the principal tensile stress originally borne by the concrete will be borne by the rebar after cracking. The amount of rebars should be sufficient to provide the necessary bearing capacity of the plate member. Based on this goal, tensile stress region reinforcement design theory puts forward a novel shear rebar reinforcement design theory using orthogonal grid shear rebar. The stress state of membrane component under external load effect is shown in Fig. 26(a), and the equivalent principal tensile stress f_1 is shown as Fig. 26(b). The contribution from concrete to resist the principal tensile stress between cracks is neglected. The principal tensile stress is solely borne by the orthogonally steel rebars after the emergence of diagonal cracks. The the balance system is built as shown in Fig. 26(c), to enable the plate element continues to bear the external load. In the infinitesimal element, the crack length is s and the principal compressive stress dip angle of concrete is θ. The horizontal component and vertical component of principal tensile stresses after cracking are respectively balanced by horizontal and vertical part of the orthogonal rebar crossing the crack surface. The corresponding balance equation (Xu and Yu 2012, Chao and Xu 2012) is

$$f_1 \times s \times b \times \cos\theta = f_{sv} \times A_{sv} \times \frac{s \times \cos\theta}{s_k} \tag{13}$$

$$f_1 \times s \times b \times \sin\theta = f_{sh} \times A_{sh} \times \frac{s \times \sin\theta}{s_h} \tag{14}$$

The reinforcement ratio of horizontal rebar and vertical rebar can be obtained by simplifying Eq. (14).

$$\frac{A_{sv}}{s_k} = \frac{f_1 b}{f_{sv}} \tag{15}$$

$$\frac{A_{sh}}{s_h} = \frac{f_1 b}{f_{sh}} \tag{16}$$

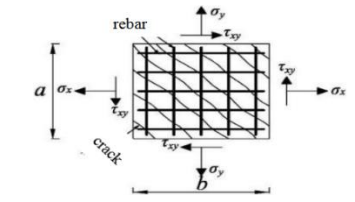

(a) Stress status thin film component

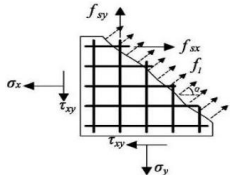

(b) Tensile stress status

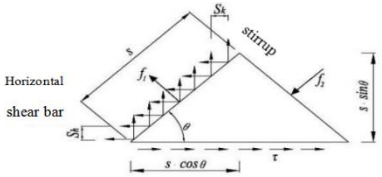

(c) Equilibrium of fracture surface

Fig. 26 Design and calculation diagram of orthogonal grid shear steel bar

In the equation, A_{sv} and A_{sh} are respectively the area of vertical stirrup and horizontal rebar, respectively. s_k and s_h are the spacing between vertical stirrup and horizontal rebar, respectively. f_{sv} and f_{sh} are the yield stress of vertical stirrup and horizontal rebar, respectively. f_1 is the principal tensile stress of concrete transferring to the rebar (Xu and Yu 2012, Chao and Xu 2012).

The tensile stress region reinforcement design method can be applied for the top and bottom slabs of girders with corrugated steel webs using the stresses obtained from the respective spatial grid model. The reinforcement design includes the in-plane vertical and horizontal reinforcement and also the the out-of-plane vertical and horizontal reinforcement.

The reinforcement amounts of each small plate of top and bottom plates are determined using the proposed method and using the tradition method based on the internal forces obtained from the spine model. The grid reinforcement design process is shown in Fig. 27. In the grid reinforcement, for the horizontal rebar, if the middle plane and the upper and lower layer rebar are reinforced in the same position, it is valued as per the maximum of in-plane principal stress horizontal reinforcement and horizontal out-of-plane reinforcement for each plate. If the middle plane is reinforced in the middle layer and the upper and lower layer rebar is reinforced at the upper and lower edge of plate, the sum of in-plane and out-of-plane reinforcement is valued. For the vertical rebar, if the middle plane and the upper and lower layer rebar are reinforced in the same position, it is valued as per the maximum of in-plane principal stress vertical reinforcement and vertical out-of-plane reinforcement for each plate. If the middle plane is reinforced in the middle layer and the upper and lower layer rebar is reinforced at the upper and lower edge

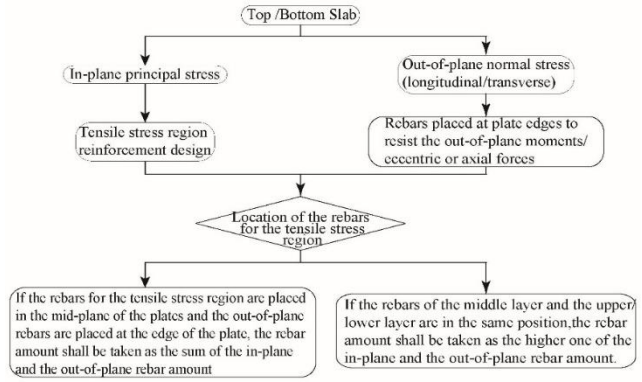

Fig. 27 Flow chart of reinforcement design for composite box girder with corrugated steel web

of plate, the sum of in-plane and out-of-plane reinforcement is valued (Xu and Yu 2012, Chao and Xu 2012).

6. Case analysis

6.1 Project overview

The superstructure of the Longhai Road bridge in Zhengzhou is studied here. The superstructure adopts the concrete box girders with corrugated steel webs. The span arrangement is 31 m + (9 × 50) m + (9 × 50 + 40) m + (3 × 26) m + (52 + 80 + 52) m + (32.061 + 32 + 31.876) m in the left range / (34.906 + 34.98 + 35.09) m in the right range. The (9 × 50) m + (9 × 50 + 40) m part is made up of continuous composite box girder with corrugated steel webs. The (9 × 50) m continuous spans are used for the following analysis, which is shown in Fig. 28.

6.2 Spatial grid model

The spatial grid model is used to analyze this structure. The full bridge includes 5,625 nodes and 12,009 elements. The external prestressing tendons are simulated by the tension-only members. In the model, the main bridge support adopts the support element. The upper node of the support element connects to the lower node of the vertical element for the cross beam. The lower node of the support element is restrained as per the boundary conditions (construction process or completed bridge state). For the selection of global coordinate system of bridge, the origin is set in the middle of end cross beam on one side, and the direction notation follows the right hand rule, i.e., x axis is in the longitudinal direction along the bridge, y axis is in the vertical direction. z axis is in the horizontal direction.

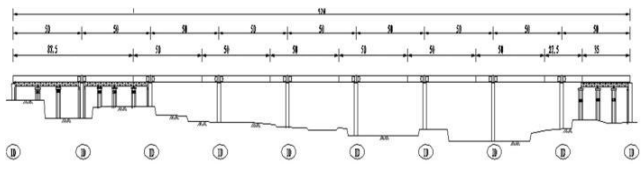

Fig. 28 Span layout (Unit: m)

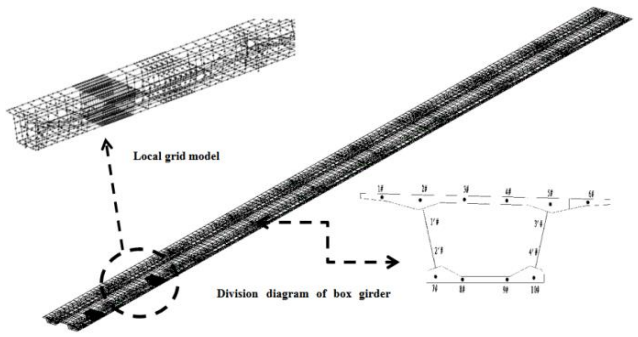

Fig. 29 Spatial grid calculation model

It is necessary to correct the longitudinal elastic modulus E_0 of the corrugated steel web, and adopt the effective elastic modulus Ex. The corrugated steel web of the structure adopts two types of thickness of t = 16 mm and t = 20 mm. When t = 16 mm, the values of the longitudinal effective elastic modulus E_X and the original elastic modulus E_0 satisfy $Ex/E_0 \approx 500$. When t = 20 mm (only adopted by the span end pivot overlapping section at both sides, with length range of 4.65m), it is obtained that $Ex/E_0 \approx 320.1$. In the spatial grid model, the longitudinal rigidities of the longitudinal element representing the corrugated steel webs are modified correspondingly. The reductions of 1/500 and 1/320.1 are made on the axial areas of these longitudinal elements having the thickness t = 16 mm and t = 20 mm, respectively. Other geometrical properties and material parameters shall not be corrected. The spatial grid model is shown in Fig. 29.

6.3 Reinforcement calculation results

To check the design result of the tensile stress region reinforcement, the reinforcement design at the middle and the over pier cross section of the side span, and the key plates 2#, 3#, 7# and 8# in Fig. 11(c) are studied. To demonstrate the economy and effectiveness of the proposed method in composite box girder with corrugated steel webs, the reinforcement design result using the proposed method is compared with the result using the internal forces obtained from spine model and the one used in the blueprint.

(1) Transverse section reinforcement

The spatial grid model divides the top and bottom plates into in-plane and out-of-plane reinforcement. This model has considered the horizontal effect of bridge deck, without calculating the bridge deck reinforcement separately. The single girder method only places the out-of-plane vertical reinforcement for tensile region. Figs. 30~33 indicate the comparison results of side span 1/2L grid, blueprint, single girder reinforcement and web stress, respectively. Figs. 34~37 indicate the comparison results of central pivot grid of side span, blueprint, single girder reinforcement and web stress, respectively.

According to the vertical reinforcement design for top slabs from the tensile stress region method, single girder and blueprint in Fig. 30, the reinforcement amount from the

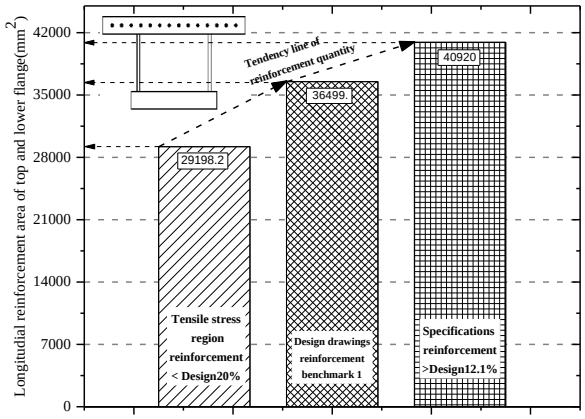

Fig. 30 Longitudinal reinforcement comparison of top slab

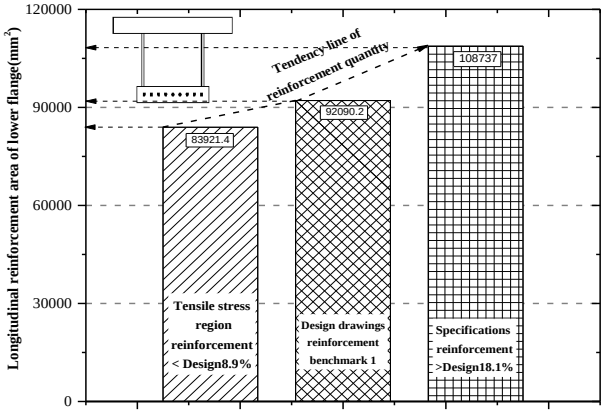

Fig. 31 Longitudinal reinforcement comparison of bottom slab

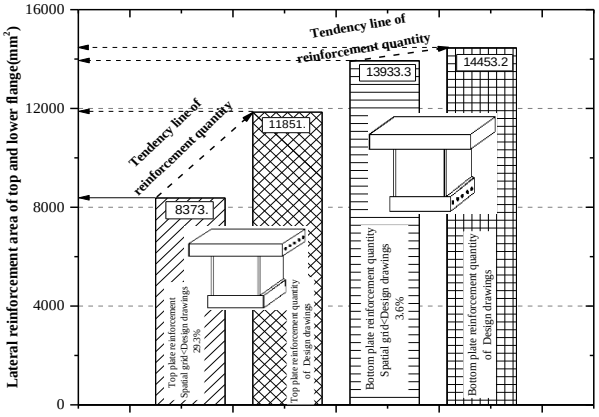

Fig. 32 Transverse reinforcement comparison of top and bottom slab

tensile stress region method is less than that of blueprint by 20%. The standard single girder reinforcement amount is more than that of blueprint by 12.1%, and the reinforcement amount of spatial gird is less than that f standard single girder reinforcement amount by nearly 30%. According to the vertical reinforcement results for bottom slabs from the tensile stress region, single girder and blueprint in Fig. 31, the reinforcement amount from the tensile stress region method is less than that of blueprint by 8.9%, and the standard single girder reinforcement amount is more than that of blueprint by 18.1%, and the reinforcement amount of spatial gird is less than that of standard single girder reinforcement amount by nearly 26%. According to the horizontal reinforcement results for top and bottom slabs from the tensile stress region method and blueprint in Fig. 32, the transverse reinforcement amount for top slabs from the tensile stress region method is less than that of blueprint by 29.3%, and the transverse reinforcement amount for bottom slabs from the tensile stress region method is less than that of blueprint by 3.6%.

According to the longitudinal reinforcement design of top slabs from the tensile stress region, single girder and blueprint in Fig. 34, the reinforcement amount of spatial gird is less than that of blueprint by 33.7%, and the standard single girder reinforcement amount is more than that of blueprint by 43.8%. Meanwhile, the reinforcement amount of spatial gird is less than that of standard single girder reinforcement amount by nearly 70%. According to the longitudinal reinforcement design of bottom slabs from the tensile stress region, single girder and blueprint in Fig. 35, the reinforcement amount of spatial gird is less than that of blueprint by 25.8%, and the standard single girder reinforcement amount is more than that of blueprint by 12.4%. Meanwhile, the reinforcement amount from the tensile stress region method is less than that of standard single girder reinforcement design by nearly 13%. The

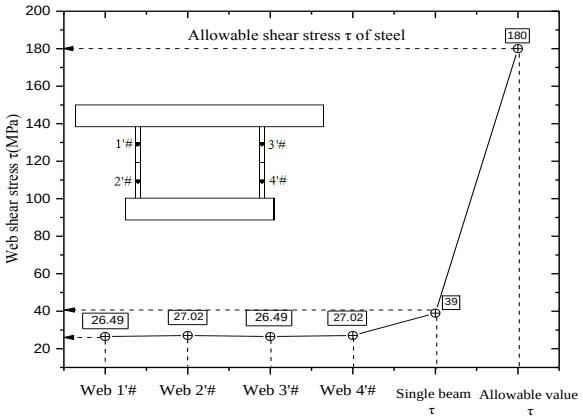

Fig. 33 Shear stress comparison of web

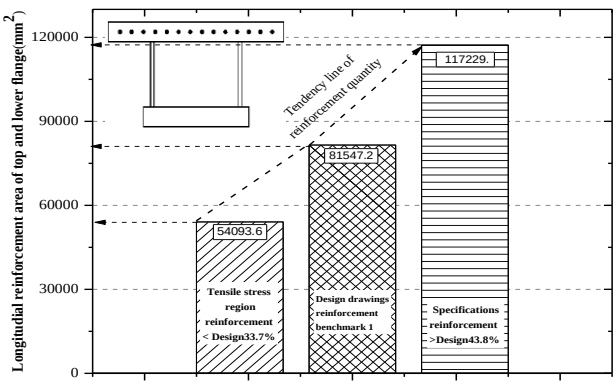

Fig. 34 Longitudinal reinforcement comparison of top slab

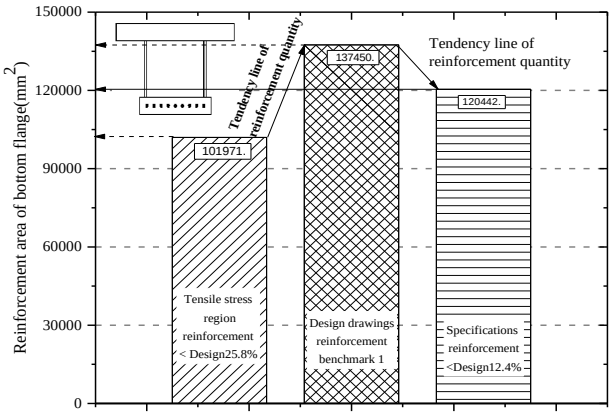

Fig. 35 Longitudinal reinforcement comparison of bottom slab

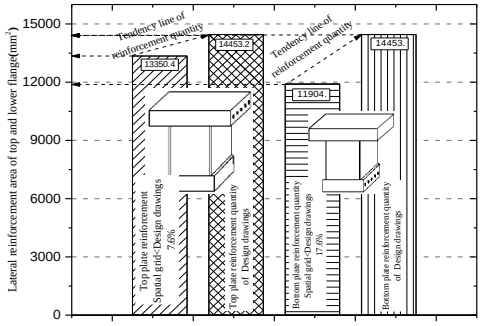

Fig. 36 Transverse reinforcement comparison of top and bottom slab

reinforcement amount from the tensile stress region method is the minimum. According to the transverse reinforcement design for top and bottom slabs of spatial grid model and blueprint in Fig. 36, the transverse reinforcement amount for the top slabs from the tensile stress region method is less than that of blueprint by 7.6%. Also, the transverse reinforcement amount for the bottom slabs from the tensile stress region method is less than that of blueprint by 17.6%.

The single girder model fails to calculate the transverse rebar of bridge deck, and shall be completed by means of

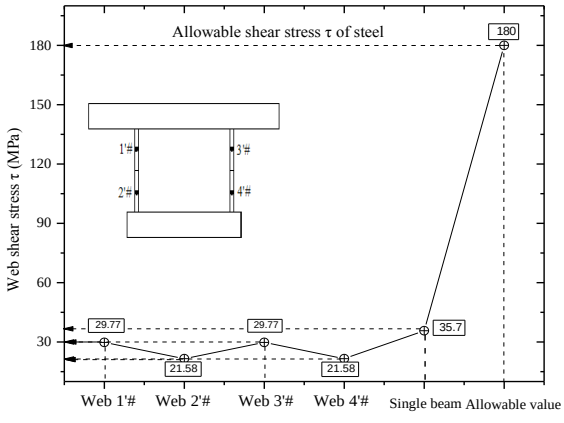

Fig. 37 Shear stress comparison of web

finite element model of space. The vertical and horizontal reinforcement amount of top and bottom plates arranged in the spatial grid is less than the reinforcement amount of blueprint and standard single gird, and the reinforcement amount of standard single girder is generally larger. However, based on the stress reinforcement, the reinforcement project is considered to be relatively comprehensive and clearly calculated, and the reinforcement is the tensioned rebar.

By the comparison results of web stress diagram in Figs. 33 and 37, the spatial grid model can extract the shear stress value at different points along the web height direction, showing the distribution trend of shear stress height direction of steel web. The single girder calculation result is a average shear stress value, and the magnitude is slightly more than the spatial grid model calculation result, but two calculation results are less than the shearing strength design value of rolled steel.

(2) Transverse reinforcement amount for the key plates in longitudinal elements

Plate 2#, 3#, 7# and 8# are key positions of box girder section. The in-plane and out-of-plane reinforcement amount trend line is drawn along the longitudinal direction along the span. The reinforcement trend line of Plate 2#, 3#, 7# and 8# is shown as Figs. 38~41, respectively.

Plate 2# and 3# on the section are located at top slabs, and Plate 7# and 8# are located at bottom slabs. From Figs. 38~41, sudden changes of the reinforcement amount of Plate 2# and 3# are observed at the negative moment region at piers.

On the contrast, sudden changes of the reinforcement amount of Plate 7# and 8# are observed at the positive moment region at midspan. The reinforcement trend line of Plate 2#, 3#, 7# and 8# is basically consistent with the

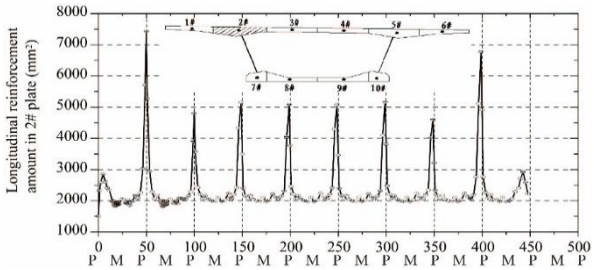

Fig. 38 Longitudinal reinforcement trend line across the span of 2# slab (P for piers, M for midspan)

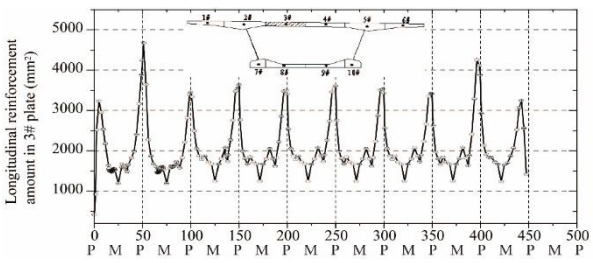

Fig. 39 Longitudinal reinforcement trend line across the span of 3# slab (P for piers, M for midspan)

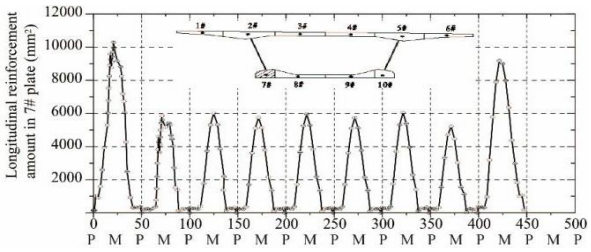

Fig. 40 Longitudinal reinforcement trend line across the span of 7# slab (P for piers, M for midspan)

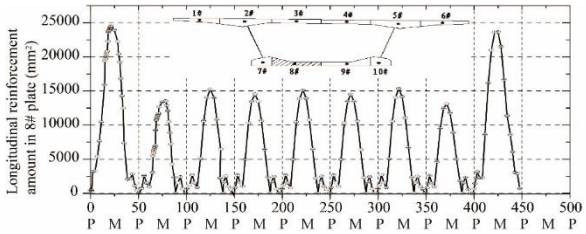

Fig. 41 Longitudinal reinforcement trend line across the span of 8# slab (P for piers, M for midspan)

moment diagram of continuous girder.

During the actual reinforcement design, the reinforcement amount for top or bottom slabs can refer to the reinforcement trend line along the span. The segment reinforcement between girder spans is conducted according to the segment reinforcement amount. The maximum value of the reinforcement trend line can be taken as a constant arrangement for the whole span to facilitate the construction.

At the research stage, it is generally recognized that the blueprint and standard single girder reinforcement is on the upper and lower edges of the slabs, while the ideal position of in-plane grid reinforcement is located at the mid-plane of the slabs. The location of the out-of-plane longitudinal and transverse reinforcement is determined according to the external force. In addition to the requirements of stress state of these structural members, it is necessary to conform to the regulations on reinforcement detailing for top and bottom slabs in highway bridge codes.

From the overall reinforcement trend line of the whole bridge, the reinforcement amount of each section and each segment is expressed clearly. This indicates that the spatial grid model and the tensile stress region method have the applicability to the overall reinforcement design of 9×50m continuous composite box girder with corrugated steel webs.

7. Conclusions

This paper describes the shortcomings of current design calculation method and reinforcement design method of composite girders with corrugated steel webs. The spatial grid model and the reinforcement design using tensile stress region method are presented. The accuracy and applicability of spatial grid model in analyzing composite girders with corrugated steel webs was first validated by a 20-m simply-supported girder. In a 9 × 50 m prestressed concrete composite continuous box girder bridge with corrugated steel webs, reinforcement arrangement was designed according to different methods.

For the longitudinal reinforcement rebars in the top and bottom slabs, the reinforcement amount designed according to the Chinese code is slightly more than the reinforcement designed by tensile stress theory or those from the blueprint. The reinforcement design according to the tensile stress region method is the minimum among them. In general, the reinforcement amount according to the Chinese code using the internal forces obtained from beam model is higher than the reinforcement amount obtained from the tensile stress region method. For the transverse reinforcement of top and bottom plates, the single girder model fails to calculate the transverse rebar of bridge deck, and shall be supplemented by additional finite element analysis. The reinforcement amount of transverse rebars of top and bottom slabs in the blueprint is more than the reinforcement amount from the tensile stress region method. Thus, the following conclusions are drawn.

- The reinforcement design of composite box girder with corrugated steel webs is proposed based on the spatial grid model and tensile stress region method. It realizes the refined reinforcement design for the in-plane and out-of-plane reinforcement in the top and bottom slabs of composite girder bridge with corrugated steel webs.
- The comparison results between the spatial grid model and the FEM using shell and solid elements verifies the accuracy of the spatial grid model in simulating the composite box girder with corrugated steel webs.
- The spatial grid model and the reinforcement design based on tensile stress region method provide a new direction for the refined design of composite box girder with corrugated steel webs.

Acknowledgments

This study was funded by Young Elite Scientists Sponsorship Program by China Association for Science and Technology. The authors thank the anonymous reviewers and the Editor for their constructive comments and advice, which greatly improved the quality of this paper.

References

Chao, L. and Xu, D. (2012), "Influence of cracking on deflections of concrete box girder bridges", *Baltic J. Road Bridge Eng.*, **7**(2), 104-111.

Chen, Y., Dong, J. and Xu, T. (2018), "Composite box girder with corrugated steel webs and trusses – a new type of bridge structure", *Eng. Struct.*, **166**, 354-362. https://doi.org/10.1016/j.engstruct.2018.03.047

Elkawas, A.A., Hassanein, M.F. and El-Boghdadi, M.H. (2017), "Numerical investigation on the nonlinear shear behaviour of high-strength steel tapered corrugated web bridge girders", *Eng.*

Struct., **134**, 358-375. https://doi.org/10.1016/j.engstruct.2016.12.044

Elkawas, A.A., Hassanein, M.F. and Elchalakani, M. (2018), "Lateral-torsional buckling strength and behaviour of high-strength steel corrugated web girders for bridge construction", *Thin-Wall. Struct.*, **122**, 112-123. https://doi.org/10.1016/j.tws.2017.10.021

Gajdzicki, M., Perliński, W. and Michalak, B. (2018), "Stability analysis of bi-directionally corrugated steel plates with orthotropic plate model", *Eng. Struct.*, **160**, 519-534. https://doi.org/10.1016/j.engstruct.2018.01.057

Hassanein, M.F. and Kharoob, O.F. (2014), "Shear buckling behavior of tapered bridge girders with steel corrugated webs", *Eng. Struct.*, **74**, 157-169. https://doi.org/10.1016/j.engstruct.2014.05.021

Jiao, P., Borchani, W., Soleimani, S. and McGraw, B. (2017), "Lateral-torsional buckling analysis of wood composite i-beams with sinusoidal corrugated web", *Thin-Wall. Struct.*, **119**, 72-82. https://doi.org/10.1016/j.tws.2017.05.025

Ko, H.J., Moon, J., Shin, Y.W. and Lee, H.E. (2013), "Non-linear analyses model for composite box-girders with corrugated steel webs under torsion", *Steel Compos. Struct., Int. J.*, **14**(5), 409-429. https://doi.org/10.12989/scs.2013.14.5.409

Li, G.Q. and Wang, W.Y. (2013), "A simplified approach for fire-resistance design of steel-concrete composite beams", *Steel Comp. Struct., Int. J.*, **14**(3), 295-312. https://doi.org/10.12989/scs.2013.14.3.295

Liu, X.G., Fan, J.S., Nie, J.G., Bai, Y., Han, Y.X. and Wu, W.H. (2015), "Experimental and analytical studies of prestressed concrete girders with corrugated steel webs", *Mater. Struct.*, **48**(8), 2505-2520. https://doi.org/10.1617/s11527-014-0334-3

Lopes, G.C., Couto, C., Real, P.V. and Lopes, N. (2017), "Elastic critical moment of beams with sinusoidally corrugated webs", *J. Constr. Steel Res.*, **129**, 185-194. https://doi.org/10.1016/j.jcsr.2016.11.005

Ma, Y., Ni, Y.S., Xu, D. and Li, J.K. (2017), "Space grid analysis method in modelling shear lag of cable-stayed bridge with corrugated steel webs", *Steel Compos. Struct., Int. J.*, **24**(5), 549-559. https://doi.org/10.12989/scs.2017.24.5.549

Pipinato, A. (2016), Innovative Bridge Design Handbook, Innovative Bridge Design Handbook. https://doi.org/10.1016/c2013-0-13492-7

Shon, S., Yoo, M., Kang, J. and Lee, S (2015), "Minimum weight design of sinusoidal corrugated web beam using differential evolution algorithm", *Int. J. Steel Struct.*, **15**(1), 213-225. https://doi.org/10.1007/s13296-015-3016-2

Tomàs, D., Lozano-Galant, J.A., Ramos, G. and Turmo, J. (2018), "Structural system identification of thin web bridges by observability techniques considering shear deformation", *Thin-Wall. Struct.*, **123**(2), 282-293. https://doi.org/10.1016/j.tws.2017.11.017

Xu, D. and Yu, Z. (2012), "Application of spatial grid model in structural analysis of concrete box girder bridges", *Proceedings of the 18th Congress of IABSE*, In: *International Association for Bridge and Struct. Eng.*, Seoul, Korea, September, pp. 2009-2016.

Xu, D., Ni, Y. and Zhao, Y. (2015), "Analysis of corrugated steel web beam bridges using spatial grid modelling", *Steel Compos. Struct., Int. J.*,**18**(4), 853-871. https://doi.org/10.12989/scs.2015.18.4.853

Xu, D., Lei, J. and Turmo, J. (2017), "Simulating composite bridges with corrugated steel webs using spatial grid model", *IABSE Symposium Report*; International Association for Bridge and Structural Engineering, Vol. 109, No. 68, pp. 230-237.

Zevallos, E., Hassanein, M.F., Real, E. and Mirambell, E. (2016), "Shear evaluation of tapered bridge girder panels with steel corrugated webs near the supports of continuous bridges", *Eng. Struct.*, **113**, 149-159. https://doi.org/10.1016/j.engstruct.2016.01.030

CC